JPhys Energy

TOPICAL REVIEW • OPEN ACCESS

Latest progress in g-C_3N_4 based heterojunctions for hydrogen production via photocatalytic water splitting: a mini review

To cite this article: Baker Rhimi *et al* 2020 *J. Phys. Energy* **2** 042003

Journal of Physics: Energy

Topical Review

Latest progress in g-C_3N_4 based heterojunctions for hydrogen production via photocatalytic water splitting: a mini review

Baker Rhimi[1], **Chuanyi Wang**[1] and **Detlef W Bahnemann**[2,3]

[1] College of Environmental Science and Engineering, Shaanxi University of Science and Technology, Xi'an 710021, People's Republic of China
[2] Laboratory of Photoactive Nanocomposite Materials, Saint-Petersburg State University, Ulyanovskaya str. 1, Peterhof, Saint-Petersburg 198504, Russia
[3] Institut für Technische Chemie, Gottfried Wilhelm Leibniz Universität Hannover, Callinstrasse 3, D-30167, Hannover, Germany

E-mail: wangchuanyi@sust.edu.cn

Keywords: hydrogen production, g-C_3N_4, heterojunction, Z-scheme, S-scheme, schottky junction

OPEN ACCESS

RECEIVED
11 May 2020

REVISED
16 August 2020

ACCEPTED FOR PUBLICATION
11 September 2020

PUBLISHED
7 October 2020

Abstract

Graphitic carbon nitride based heterojunction photocatalysts have gained increasing attention in producing the clean energy source of hydrogen. Coupling carbon nitride (g-C_3N_4) with other semiconductor materials or metals as co-catalysts is considered as an effective strategy to overcome the drawbacks of g-C_3N_4 such as the quick recombination of photogenerated charges. In this review, the recent research advancements in the construction of g-C_3N_4-based heterojunctions as well as their different charge separation/transfer mechanisms will be systematically discussed, making special emphasis on the design and fabrication of type-II, Z-scheme, S-scheme and Schottky heterojunctions and their application towards H_2 generation from water splitting. Finally, a summary and some crucial issues, which should be further resolved for developing advanced g-C_3N_4-based heterojunction photocatalysts, are presented.

1. Introduction

The increased demand for more energy as well as the environmental pollution issues due to fossil fuels consumption are among the major problems faced by humanity in the 21st century. Thus, it is necessary to explore new energy resources that are clean and eco-friendly to replace traditional fossil fuels [1]. At present, photocatalytic hydrogen (H_2) production via water splitting is an effective remedy to overcome the energy and environmental issues [2, 3]. Since the Fujishima-Honda report in 1972 on photoelectrochemical H_2 evolution [4], photocatalytic water splitting based on photoactive material has attracted considerable interdisciplinary attention. Although a plethora of potential semiconductor photocatalysts such as TiO_2, WO_3 and CdS have been extensively employed [5–8], there is still no available photocatalytic material that meets the specific requirements such as cost-effective and high efficiency for the commercial applications of photocatalytic H_2 generation via water splitting process [9, 10]. Therefore, the development of low-cost and highly effective semiconducting materials is necessary for practical applications.

Over the past few years, graphitic carbon nitride (g-C_3N_4), a 2D-structured metal-free semiconductor, has attracted increasing attention as one of the most promising photocatalytic systems for H_2 production [11–13]. The structure of g-C_3N_4 consists of a long pair of N-atom-based triazine (C_6N_7) and tri-s-triazine (C_3N_3) tectonic units and both the N-atoms in these two rings are sp^2 hybridized (figures 1(a) and (b)). It can be synthesized by direct condensation of low-cost N-rich feedstocks, including melamine [14, 15], urea [16, 17], thiourea [18] and cyanamide [19, 20]. In recent years, various methods have been effectively used in the preparation of g-C_3N_4 such as thermal polycondensation, chemical or physical vapor deposition, solvothermal synthesis and microwave heating. Among them, microwave heating technique with such advantages as time saving, low energy consumption and high economic feasibility is more effective and reliable. Remarkably, the microwave-synthesized g-C_3N_4 revealed higher thermal stability, larger surface area and stronger emission intensity than traditional preparation methods. By contrast with the widely used

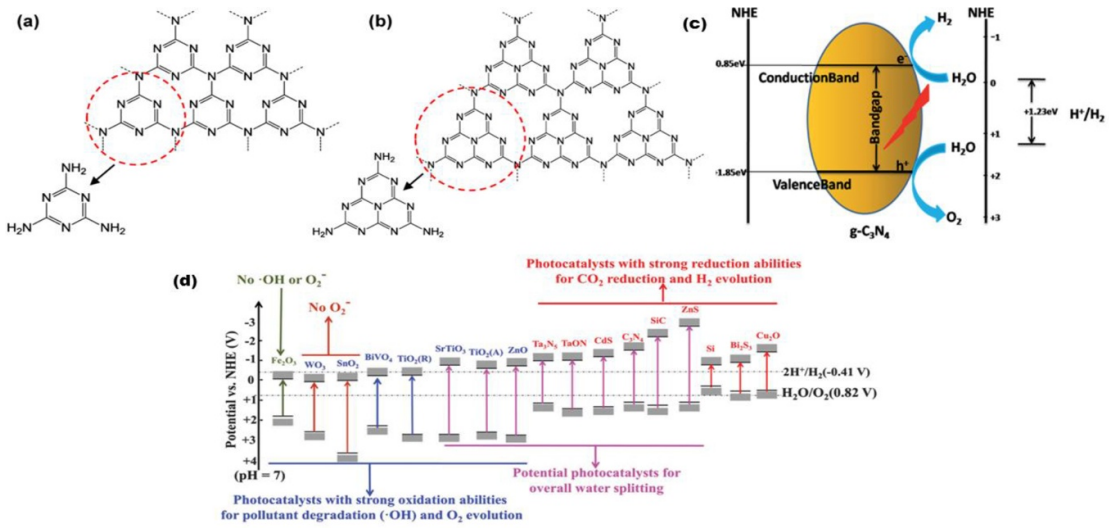

Figure 1. (a) s-triazine, (b) tri-s-triazine structures of g-C_3N_4 (adapted from Ong *et al*) [34], (c) Charge transfer mechanism over pure g-C_3N_4 (adapted from Patnaik *et al*) [9], (d) Band structures of some typical semiconductor materials (adapted from Li *et al*) [35].

photocatalyst titanium dioxide, g-C_3N_4 possess a mild band gap of 2.7 eV [21], rendering it a fascinating visible-light driven photocatalyst. Under irradiation, g-C_3N_4 is directly excited by absorbing photons with energy $\geqslant$e.g. (band gap = 2.7 eV), resulting in the creation of photogenerated electron-hole owing to the transfer of electron from the valence band (VB) to the conduction band (CB) of g-C_3N_4. The photoinduced electrons and holes act as reactive species that are highly oxidizing and reducing. They may recombine or migrate to the active sites on the surface, thereby splitting the water into oxygen and hydrogen (figure 1(c)). Despite its good photoresponse to visible light as well as its high thermal and chemical stabilities, pristine g-C_3N_4 still does not meet the requirements of a wider range of applications because of its low surface area, fast recombination and low migration ability of its photoexcited charges [22, 23]. Hence, significant efforts have been made to improve the photocatalytic efficiency of pristine carbon nitride such as doping with other elements [24–26], introducing defects [27, 28] and combining with other materials to form heterojunction interfaces [29–33].

To achieve overall water splitting, the band structure of a semiconducting material should meet specific requirements. The VB maximum level must be higher than the oxidation potential of water ($E_{O2/H2O}$, 1.23 V *vs.* NHE) and the minimum position of the CB must be more negative than the reduction potential of hydrogen ($E_{H2/H2O}$, 0 V *vs.* NHE) [36]. Hence, the semiconductor should have a bandgap higher than 1.23 eV to meet the minimum dynamic requirement. Nevertheless, in practice, water-splitting reaction requires higher energy (1.8 eV) due to overpotentials for hydrogen and oxygen evolution reactions, which greatly limits the utilization of a broad solar light spectrum. Therefore, it is hard to achieve a reasonable water splitting efficiency with a single semiconductor. Up to now, there are only a few examples of single materials that could achieve the two half-reactions (O_2 and H_2 evolution) (figure 1(d)). Owing to its suitable band gap as well as CB and VB levels, pristine g-C_3N_4 could achieve the full water splitting under visible light. Nevertheless, its photocatalytic water splitting efficiency was still unsatisfactory. Actually, the formation of heterojunctions by coupling g-C_3N_4 with other semiconductors or metals as co-catalysts is considered as an effective strategy for improving its photocatalytic properties since the heterojunction formation with suitable band alignment could realize better visible light-absorption and promote the separation/transfer of photoexcited charge carriers.

In recent years, several excellent review papers on g-C_3N_4-based materials dealing with the design of pure g-C_3N_4 and its promising photocatalytic applications have been published [34, 37–39], whereas, there are few review papers that report the application of g-C_3N_4 based heterojunctions (CNBH) and their role in improving the photocatalytic hydrogen generation process. Therefore, this review will focus on the latest development in the application of CNBH for hydrogen production via photocatalytic water splitting. In particular, the construction and the advantages and disadvantages of different CNHB, including g-C_3N_4/semiconductor and g-C_3N_4/metal systems are emphasized.

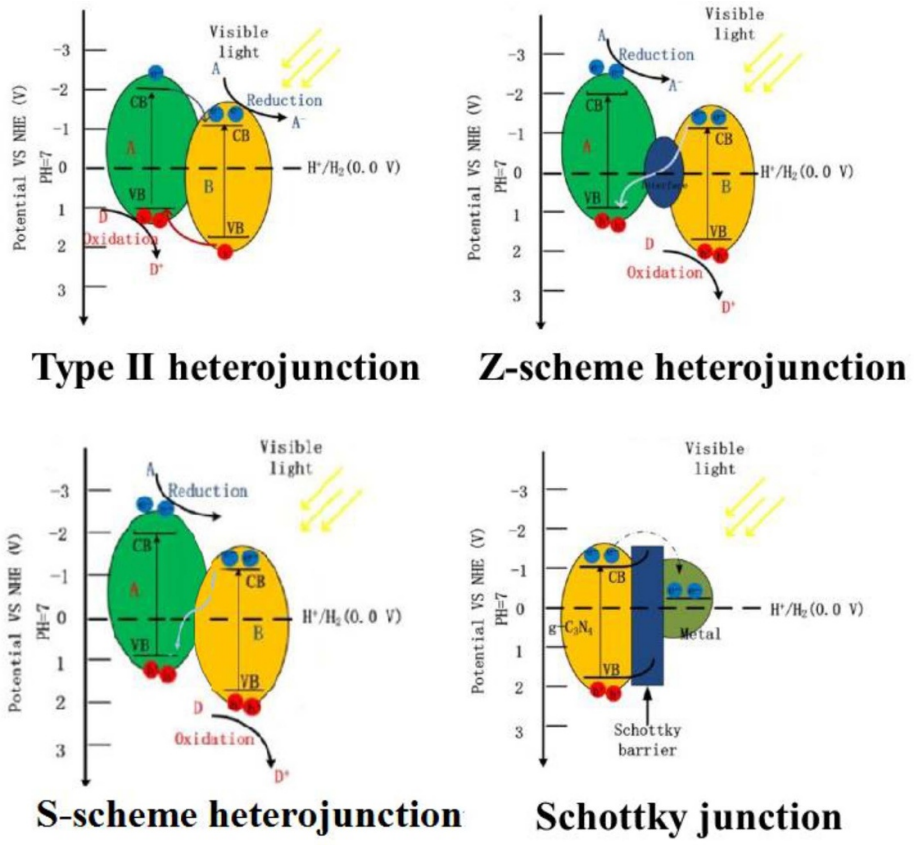

Figure 2. Charge-transfer mechanisms for g-C_3N_4-based heterojunction systems (adapted from Huang *et al*) [42].

2. Different types of g-C_3N_4-based heterojunctions

The construction of composites/heterojunctions is considered as the most viable method to improve the charge separation/transfer process and thereby increasing the overall photocatalysis efficiency. Due to its appealing physico-chemical properties, many metal nanoparticles and semiconductors could easily be combined with g-C_3N_4 semiconductor. Coupling g-C_3N_4 and other semiconducting materials with different favorable properties induces the creation of band bending at the interface of the heterojunction with an inner electric field so that the transfer and the separation of free charges can be significantly improved [40–42]. In general, CNBH systems could be divided into four main categories, e.g. type II heterojunction, Z-scheme heterojunction, S-scheme heterojunction and Schottky junction (figure 2). The following section will summarize and discuss the latest advances in CNBH systems for photocatalytic hydrogen production.

2.1. Type II heterojunctions

For the most CNBH systems, type II heterojunction is the most common type. As displayed in figure 2, type II heterojunction is commonly formed by the combination of two semiconductors (SC 1 and SC 2) possessing wide and small band gaps; among them one must has a more negative CB level. Upon light irradiation, when the CB and VB levels of SC 1 are greater than the CB and VB positions of SC 2, photogenerated holes (h^+) migrate from the VB of SC 2 to the VB of SC 1, meanwhile photexcited electrons (e^-) migrates from the CB of SC 1 to the CB of SC 2. In this way, the transfer of photoinduced e^- and h^+ in opposite directions results in an efficient charge separation, which greatly enhance the photocatalytic efficiency.

Recently, many efforts have been invested for preparing C_3N_4-based type II heterojunctions for photocatalytic H_2 production. In principle, the band alignment and the close interface contact between the different semiconductors are the crucial factors for the fabrication of an efficient type II heterojunction photocatalysts [43]. Shen *et al* [44] synthesized Black TiO_2 nanobelts/g-C_3N_4 (b-TiO_2/g-C_3N_4) type II heterojunction by hydrothermal-calcination method. The formation of laminated heterojunctions was clearly demonstrated by SEM and TEM results, which show that g-C_3N_4 surfaces are coated of TiO_2 nanobelt (figures 3(a)–(c)). The intimate contact between b-TiO_2 and g-C_3N_4 promotes the charge separation in the

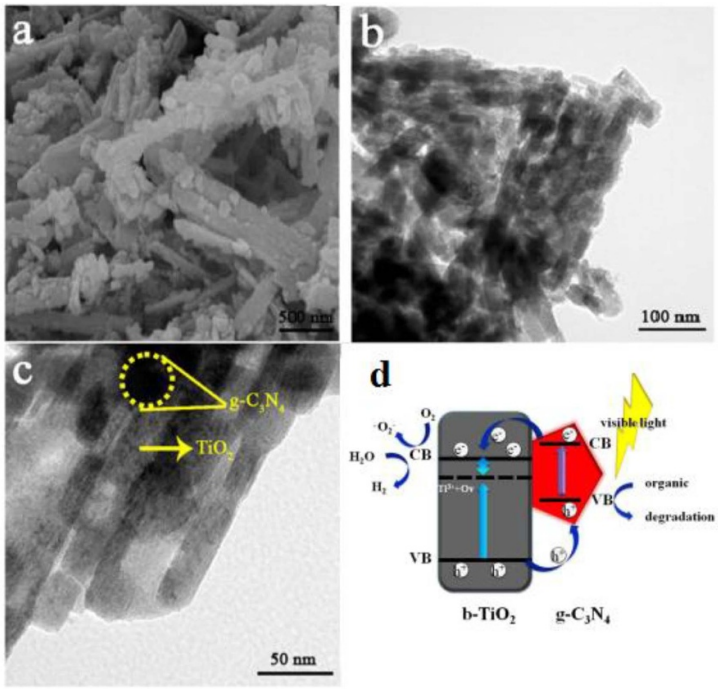

Figure 3. (a) SEM image of TiO_2/g-C_3N_4, (b, c) TEM images of TiO_2/g-C_3N_4, (d) The charge separation pathway in TiO_2/g-C_3N_4 photocatalyst (adapted from Shen *et al*) [44].

b-TiO_2/g-C_3N_4 photocatalyst (figure 3(d)), resulting in superior H_2 generation activity compared to single semiconductors g-C_3N_4 and TiO_2. Lin *et al* [45] investigated the electronic and optical properties of g-C_3N_4/TiO_2 type II heterojunction photocatalyst using density-functional theory (DFT) calculations to understand the mechanism behind its enhanced H_2 production activity. The calculation results of TDOS and PDOS (figures 4(a)–(c)) indicated that the close contact between the two components leads to band gap narrowing, which improves the visible light-harvesting of g-C_3N_4/TiO_2. The results show that the VBM of the g-C_3N_4/TiO_2 system is dominated by C 2p and N 2p states instead of O 2p states for the TiO_2, which reduces its bang gap, while the CBM of g-C_3N_4/TiO_2 system is occupied by Ti 3d states (figure 4(d)). Interestingly, the CBM and VBM of TiO_2 are lower than those of carbon nitride, making the type II heterojunction feasible in g-C_3N_4/TiO_2 heterojunction. The improved photoactivity of the g-C_3N_4/TiO_2 system is due to the suitable type II band alignment structure, which promotes the e^- and h^+ separation efficiency.

In another work, Li *et al* [46] have prepared Cu_2O/g-C_3N_4 heterostructure via combined solvothermal and chemisorption process. The Cu_2O/g-C_3N_4 heterostructure showed higher photocurrent intensity compared to that of Cu_2O and pure g-C_3N_4 (figure 5(a)), indicating the high separation and transport efficiency of photoexcited species through the interfacial connection of g-C_3N_4 and Cu_2O. As displayed in figure 5(b), due to the large contact area and the intimate contact between the two semiconductors, the excited e^- on Cu_2O semiconductor could migrate to the CB of g-C_3N_4, which promotes the charge separation, resulting in superior photoactivity for H_2 production. Other semiconductors such as MoS_2 [47, 48], In_2O_3 [49], TiO_2 [50–53], ZnS [54], Bi_2MoO_6 [55], SiC [56], CeO_2 [57], CoO [58] and CdS [59, 60] have been employed to combine with g-C_3N_4 for the fabrication of advanced type II heterojunction materials with high photocatalytic efficiency (table 1).

Although all g-C_3N_4-based type II heterojunction photocatalytic materials exhibit enhanced photoactivity in H_2 production, the type II heterojunctions weakens the redox ability of e^- and h^+ because of the migration of photoinduced species to the lower-lying CB and VB [13, 77]. To surmount this shortfall of type II heterojunction, a novel type of heterojunction, named as Z-scheme heterojunction, is proposed [78]. In this new charge-transfer mechanism, the photoinduced e^- on the lower-lying CB of one SC could recombine with the photoinduced h^+ on the lower-lying VB of the other SC [79–81] (figure 2). In this way, e^- remains at the more negative CB potential and the h^+ remains at the more positive VB potential, which maintains the high redox powers of the free charge carriers. Therefore, the Z-scheme heterojunction systems can realize an effective charge transfer and separation with high redox abilities of photoinduced of e^-–h^+ pairs.

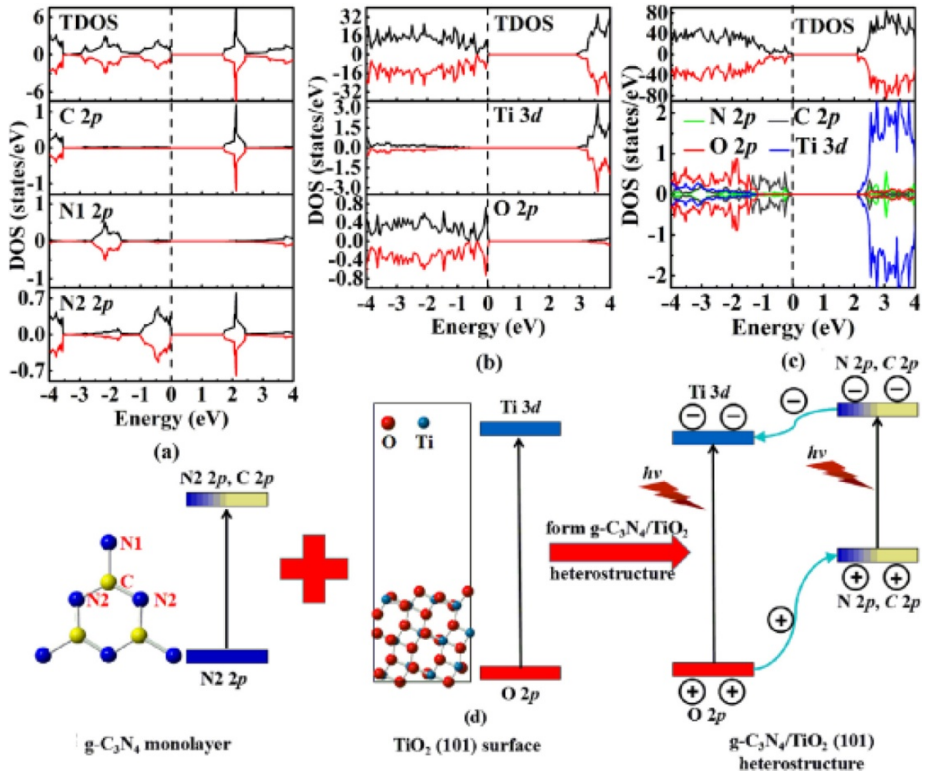

Figure 4. Calculated TDOS and PDOS of (a) g-C_3N_4, (b) TiO_2, (c) g-C_3N_4/TiO_2 heterojunction, (d) Schematic diagram of the g-C_3N_4/TiO_2 type II heterojunction system (adapted from Lin *et al*) [45].

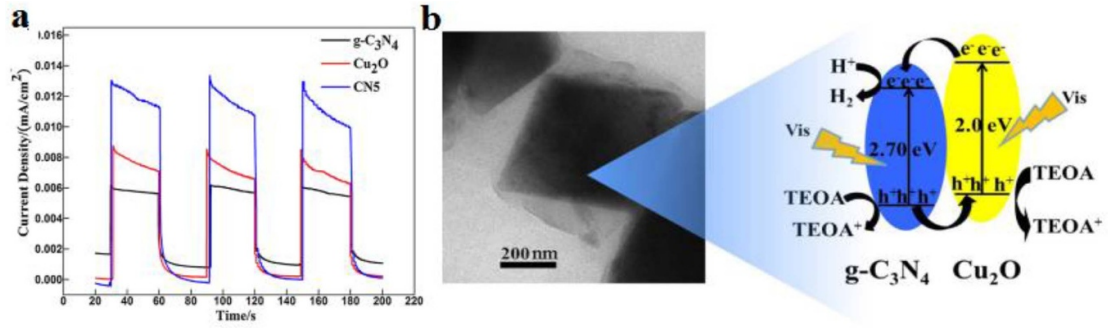

Figure 5. (a) Transient photocurrent responses of pure g-C_3N_4, Cu_2O and Cu_2O/g-C_3N_4 (CN5), (b) Schematic diagram of the charge separation/transfer pathway over Cu_2O/g-C_3N_4 (adapted from Liu *et al*) [46].

2.2. Z-scheme heterojunctions

Inspired by the natural photosynthesis system, constructing CNBH systems has emerged as a promising option to enhance the photoactivity of g-C_3N_4 in H_2 production. Figure 6 shows the typical forms of Z-scheme mechanisms with or without electron mediators. Notably, the electron mediator plays a crucial role in promoting the separation of the carriers as it affords sites for coupling photoinduced charges with weak redox ability. The original Z-scheme heterojunction system was applied in liquid phase using shuttle redox mediators including Fe^{2+}/Fe^{3+}, I^-/IO^{3-} and $[Co(bpy)_3]^{3+/2+}$ [78, 82–84]. Nevertheless, the soluble redox shuttles-mediated Z-scheme heterojunction photocatalysts are only applicable in liquid phase; hence, the development of Z-schemes with solid electron mediators is very desirable (figure 6(a)). Recently, a new mediator-free Z-scheme heterojunction system, named as direct Z-scheme, was proposed [85, 86]. Contrary to the mediated Z-scheme heterojunction system where a conductor is employed to afford sites for charge recombination and relay, in the direct Z-scheme system, the photoexcited charges on the lower-lying CB of SC 2 and VB of SC 1 can directly recombine at the interface between the two semiconductors [87–89].

Recently, many researchers have reported the use of various electron mediators, including metals and carbonaceous materials as efficient electron mediators to construct g-C_3N_4-based Z-scheme heterojunction systems with high H_2 production efficiency. Li *et al* [61] synthesized Z-scheme Ag/g-C_3N_4-Ag-Ag_3PO_4

Table 1. Photocatalytic H_2 generation over type-II and Z-scheme heterojunction systems under visible light illumination.

Heterojunction systems	Charge transfer type	H_2 production Activity (μmol h^{-1} g^{-1})	Reference (Year)
Black TiO_2/g-C_3N_4	type II	555.8	[44] (2017)
Cu_2O@g-C_3N_4	type II	265	[46] (2015)
MoS_2/g-C_3N_4	type II	23.1	[47] (2014)
TiO_2/g-C_3N_4	type II	35.44	[50] (2016)
C-TiO_2@g-C_3N_4	type II	35.6	[51] (2017)
g-C_3N_4/Ti^{3+}-TiO_2	type II	290.2	[52] (2018)
Ti^{3+} self-doping black TiO_2/g-C_3N_4	type II	808.97	[53] (2019)
In_2O_3/g-C_3N_4	type II	0.99	[49] (2014)
ZnS/g-C_3N_4	type II	713.68	[54] (2018)
Bi_2MoO_6/g-C_3N_4	type II	563.4	[55] (2017)
SiC/g-C_3N_4	type II	182	[56] (2017)
N-CeO_2/g-C_3N_4	type II	43.32	[57] (2019)
CoO/g-C_3N_4	type II	262.8	[58] (2019)
CdS quantum dots/g-C_3N_4	type II	601	[59] (2015)
Ag/g-C_3N_4-Ag-Ag_3PO_4	mediated Z-scheme	221.64	[61] (2020)
CdS/Au/g-C_3N_4	mediated Z-scheme mediated	19.02 123	[62] (2015) [63] (2017)
$Cd_xZn_{1-x}S$/Au/g-C_3N_4	Z-scheme		
g-C_3N_4/nanocarbon/$ZnIn_2S_4$	mediated Z-scheme	50.32	[64] (2015)
CdS/RGO/g-C_3N_4	mediated Z-scheme	396.04	[65] (2017)
$CoTiO_3$/g-C_3N_4	direct Z-scheme	858	[66] (2016)
g-C_3N_4/WO_3	direct Z-scheme	3120	[67] (2017)
α-Fe_2O_3/g-C_3N_4	direct Z-scheme	31 400	[68] (2017)
Nb_2O_5/g-C_3N_4	direct Z-scheme	1100	[69] (2019)
C_3N_4/$W_{18}O_{49}$	direct Z-scheme	8597	[70] (2017)
$Bi_2O_2CO_3$/g-C_3N_4	direct Z-scheme	965	[71] (2019)
2D WO_3/g-C_3N_4	direct Z-scheme	1853	[72] (2018)
$SnFe_2O_4$/g-C_3N_4	direct Z-scheme	132.5	[73] (2020)
N-ZnO/g-C_3N_4	direct Z-scheme	152.7	[74] (2019)
SnS_2/g-C_3N_4	direct Z-scheme	928	[75] (2020)
0D-ZnO/g-C_3N_4	direct Z-scheme	322	[76] (2017)

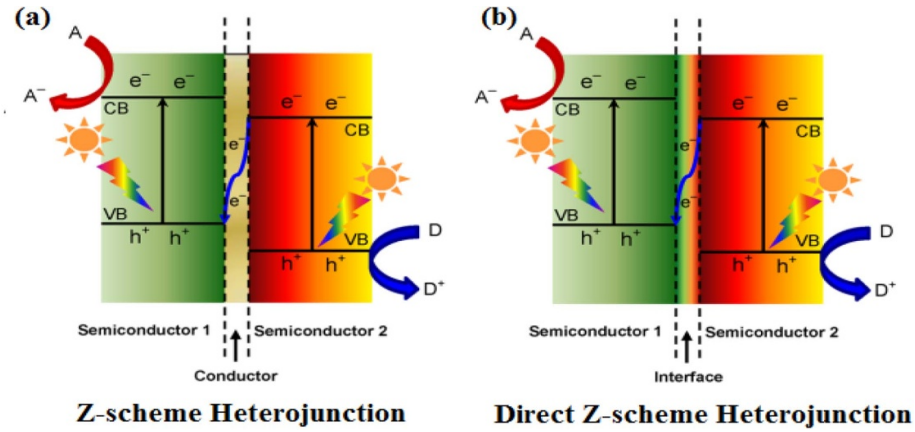

Figure 6. Various types of Z-scheme heterojunction: (a) mediated Z-scheme heterojunction, (b) direct Z-scheme heterojunction (adapted from Ong *et al*) [34].

heterostructure. In the SEM and TEM images (figures 7(a)–(c)), the Ag/g-C_3N_4-Ag-Ag_3PO_4 heterojunction can be found, where Ag NPs are lied between Ag_3PO_4 and g-C_3N_4 and also located on other side of carbon nitride. An optimal Ag/g-C_3N_4-Ag-Ag_3PO_4 heterostructure exhibited the highest hydrogen production

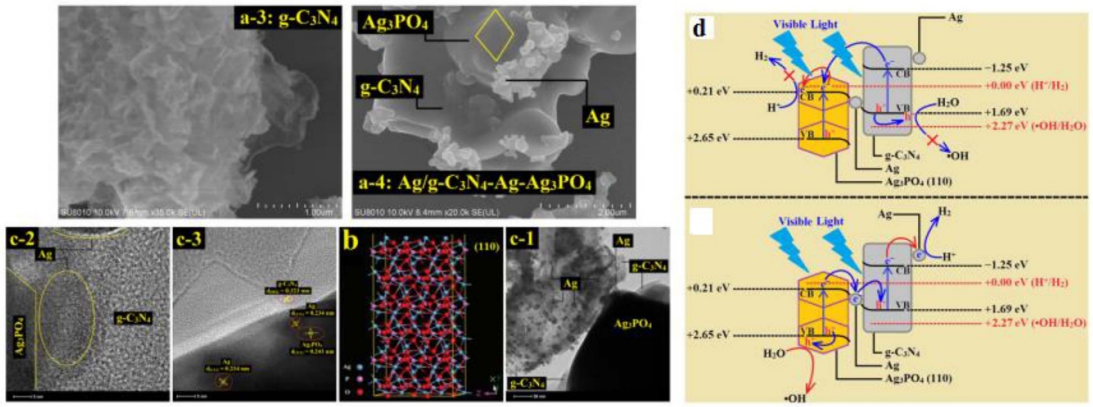

Figure 7. (a) SEM images, (b, c) TEM images of Ag_3PO_4, g-C_3N_4 and Ag/g-C_3N_4-Ag-Ag_3PO_4, (d) the possible electron transfer mechanisms in Ag/g-C_3N_4-Ag-Ag_3PO_4 photocatalyst (adapted from Li *et al*) [61].

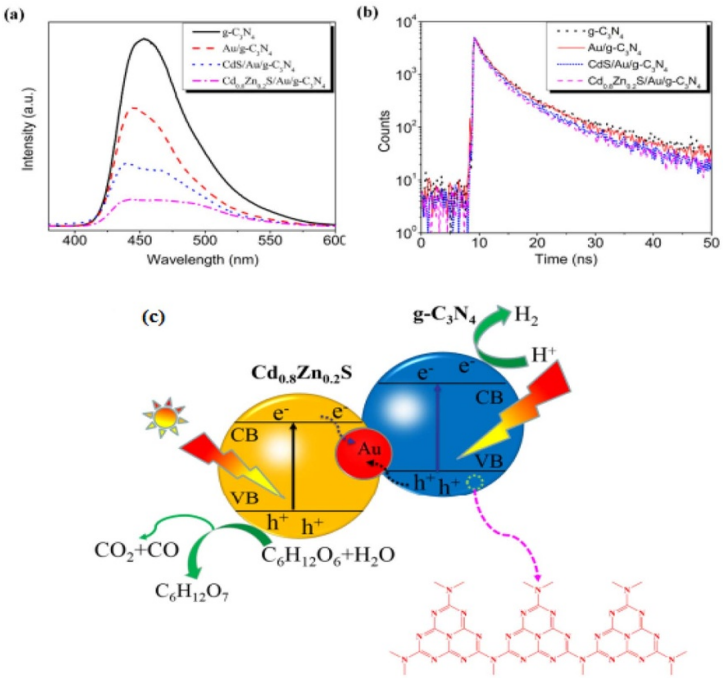

Figure 8. (a) Steady-steady PL spectra, (b) time-resolved PL spectra for g-C_3N_4, Au/g-C_3N_4 and $Cd_{0.8}Zn_{0.2}S$/Au/g-C_3N_4, (c) Possible electron transfer mechanism in $Cd_xZn_{1-x}S$/Au/g-C_3N_4 system (adapted from Zhao *et al*) [63].

(221.64 μmol) over three times that the rate of pristine g-C_3N_4. Interestingly, Ag NPs that lie between the two semiconductors promote the migration of e^- from the CB of Ag_3PO_4 to the VB of g-C_3N_4, meanwhile, Ag NPs on the other side of carbon nitride act as co-catalyst and thereby enhancing the photocatalytic efficiency (figure 7(d)). Moreover, Au is also considered as an efficient electron mediator [62, 63]. In our previous work [63], a $Cd_xZn_{1-x}S$/Au/g-C_3N_4 system was developed for photocatalytic H_2 production, which accomplished a significantly enhanced H_2 generation activity. PL spectra and time-resolved photoluminescence results (figures 8(a) and (b)) verified the efficient spatial separation of photogenerated e^- and h^+ in $Cd_xZn_{1-x}S$/Au/g-C_3N_4 photocatalysts mainly originated from the Z scheme charge flow (figure 8(c)).

Shi *et al* found that nanocarbon is an effective electron mediator in the Z-scheme g-C_3N_4/nanocarbon/$ZnIn_2S_4$ heterojunction [64]. Namely, nanocarbon could enhance the conductive capability, enhancing the charge separation/transfer process and thus improving the H_2 production activity. In another work, Jo and co-workers reported the preparation of Z-scheme CdS/RGO/g-C_3N_4 photocatalyst using RGO as electron mediator [65]. Owing to its good conductivity, RGO could accelerate the electron migration at the CdS/g-C_3N_4 interface, which resulted in high H_2 production activity.

Although their important role in promoting the spatial charge separation in Z-scheme heterojunctions, solid electron mediators have some drawbacks such as backward reactions as well as photocorrosion. In

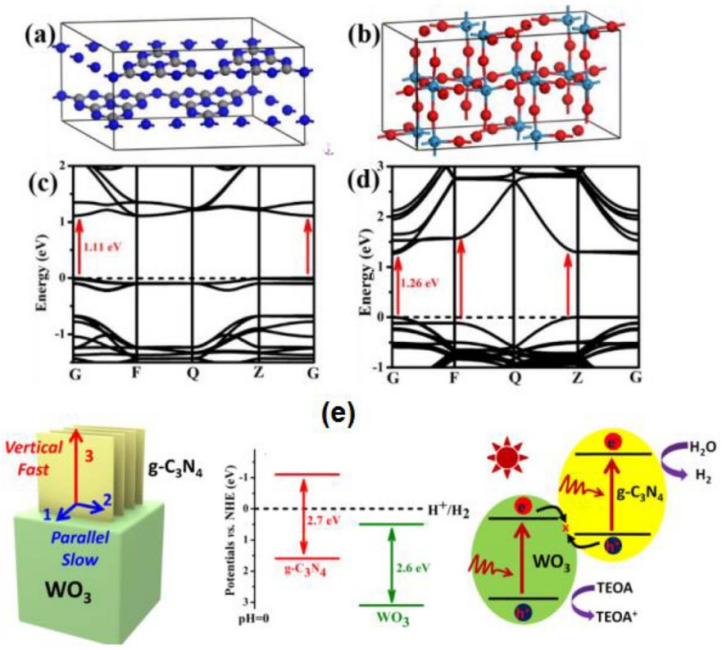

Figure 9. Crystals structures of (a) g-C_3N_4, (b) WO_3, the calculated electronic band structures of (c) g-C_3N_4, (d) WO_3, (e) The charge separation pathway in g-C_3N_4/WO_3 system (adapted from Yu *et al*) [67].

particular, it has been well established that noble metals suffer from shielding effects, which limit the photoactivity of the mediated Z-scheme systems. In regard of this, the creation of direct Z-scheme systems (figure 6(b)) is put forward, which is able to resolve the shortcomings of the mediated Z-scheme systems. The typical CNBH systems, including the mediated and direct Z-scheme systems are summarized in table 1.

It is noteworthy that the close contact between SC 1 and SC 2 in the direct Z-scheme heterojunction system plays a crucial role because the interface has the same role as the electron mediators. Hence, the effective combination of SC 1 and SC 2 is essential for preparing efficient direct Z scheme heterojunction system. Most recently, Ye *et al* [66] fabricated a direct Z-scheme $CoTiO_3$/g-C_3N_4 photocatalyst, which showed high photocatalytic hydrogen production activity of 858 μmol h^{-1} g^{-1} due to the close contact between $CoTiO_3$ and carbon nitride. In another work, Yu and co-workers [67] reported the construction of direct Z-scheme g-C_3N_4/WO_3, which showed enhanced hydrogen production rate of 3120 μmol h^{-1} g^{-1} due to the formation of internal electric fields in the heterojunction system and the covalent W-O-N-$(C)_2$, which accelerate the transfer of photoexcited carriers. Generally, it is necessary to investigate the charge transfer pathway for any heterojunction system because of the competition between Z-scheme and the type II heterojunction mechanisms. To understand the charge transfer mechanism, DFT calculations of charge carrier effective mass were conducted as depicted in figure 9. The results showed that the charge carriers in g-C_3N_4 could only move through the 2D planes, whereas electrons in WO_3 tend to move from bulk to interface and then migrate to carbon nitride, which support the direct Z-scheme mechanism (figure 9(e)).

She *et al* [68] have prepared α-Fe_2O_3/g-C_3N_4 nanocomposite with 2D/2D geometry using a small amount of α-Fe_2O_3 as a catalyst to promote the formation of ultrathin 2D g-C_3N_4 nanosheets as revealed by HRTEM and AFM measurement (figures 10(a) and (b)). The α-Fe_2O_3 nanosheets successfully formed a Z-scheme heterojunction with 2D g-C_3N_4 nanosheets owing to their matched energy levels. Interestingly, this Z-scheme junction photocatalyst showed unprecedented hydrogen generation activity of 31 400 μmol g^{-1} h^{-1} owing to the direct contact between α-Fe_2O_3 and g-C_3N_4 nanosheets, which effectively boost the e^- migration from the CB of α-Fe_2O_3 to the VB of g-C_3N_4 nanosheets (figure 10(c)). More importantly, to verify the direct Z-scheme mechanism, ESR spin-trapping experiments were performed. If the α-Fe_2O_3/g-C_3N_4 system follows the double charge transfer mechanism, e^- in the CB of g-C_3N_4 will move to the CB of α-Fe_2O_3, while the h^+ will move to the VB of g-C_3N_4. Taking into consideration the bands edge potentials of g-C_3N_4 and α-Fe_2O_3 semiconductors as well as the redox potentials of $OH^-/{}^\bullet OH$, $H_2O/{}^\bullet OH$ and $O_2/{}^\bullet O_2^-$ couples, it was deduced that the e^- in the CB of α-Fe_2O_3 cannot generate ${}^\bullet O_2^-$ radicals and the h^+ in the VB of g-C_3N_4 cannot generate hydroxyl radicals from OH^- or H_2O. However, ESR spin-trapping results (figures 10(d)–(f)) revealed that the α-Fe_2O_3/g-C_3N_4 system could generate ${}^\bullet OH$ and ${}^\bullet O_2^-$ radicals under visible light illumination, which cannot be explained by the double charge transfer pathway. Therefore, the results strongly suggest the predominance of the direct Z-scheme charge transfer

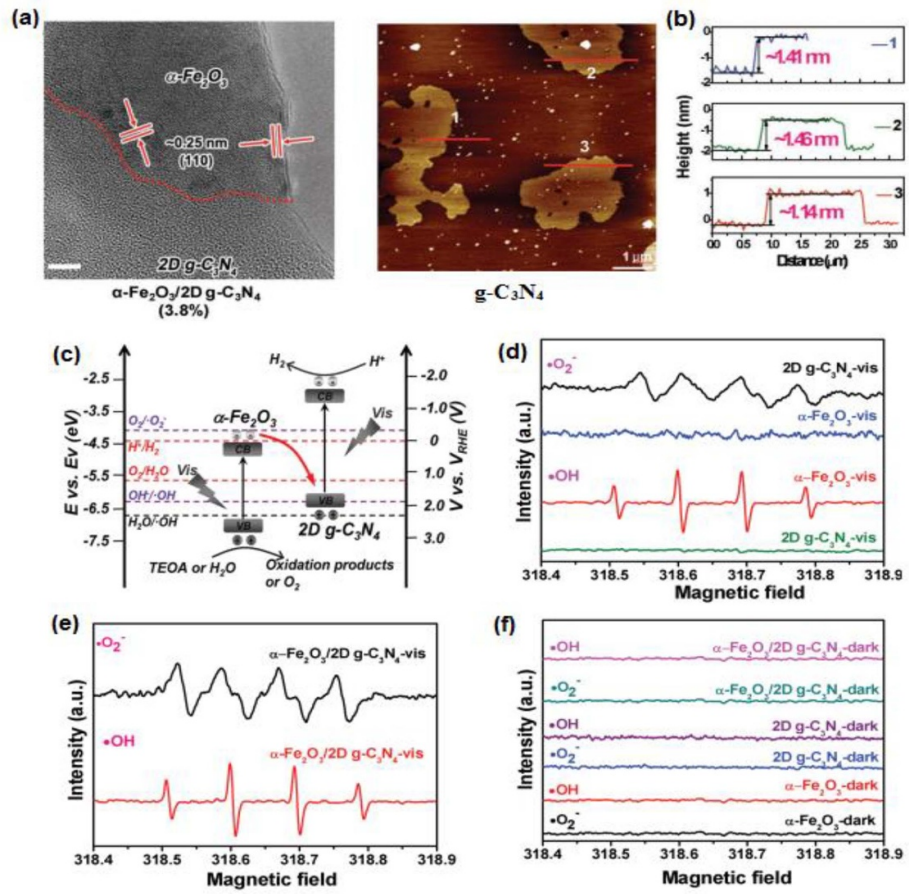

Figure 10. (a) HRTEM image of α-Fe_2O_3/g-C_3N_4, (b) AFM of pristine g-C_3N_4 nanosheet, (c) schematic diagram of the photocatalytic mechanism of α-Fe_2O_3/g-C_3N_4, (d) DMPO spin-trapping ESR spectra of α-Fe_2O_3 and g-C_3N_4, (e) DMPO spin-trapping ESR spectra of α-Fe_2O_3/g-C_3N_4 (3.8%), (f) DMPO spin-trapping ESR spectra of g-C_3N_4, α-Fe_2O_3, and α-Fe_2O_3/g-C_3N_4 (3.8%) in dark (adapted from She *et al*) [68].

pathway. Several other semiconducting materials have been coupled with carbon nitride to fabricate efficient direct Z-scheme heterojunction systems for H_2 evolution reaction, including Nb_2O_5 [69], $W_{18}O_{49}$ [70], $Bi_2O_2CO_3$ [71], 2D WO_3 [72], $SnFe_2O_4$ [73], N-ZnO [74], SnS_2 [75], 0D-ZnO [76].

2.3. S-scheme heterojunctions

As aforementioned in the previous sections, traditional type-II heterojunctions could extremely facilitate the separation of charge carriers due to staggered band alignment. However the redox ability of the photogenerated electrons and holes is weakened, which is unfavorable for photocatalytic reactions. Although, Z-scheme heterojunctions are capable of spatially separating the photoinduced charge carriers and preserving the electrons and holes with high redox ability, they still have some drawbacks. In Z-scheme heterojunction system, the conductor promotes the migration of e- from the photocatalyst with higher CB potential to the photocatalyst with lower VB potential, however, e- can also migrate through the conductor to the surface if the conductor is not situated between the two photocatalysts. Thus, the charge transfer pathway in Z-scheme heterojunction system might be different from what it is claims to be. In order to overcome the shortcomings of Z-scheme mechanism, a new step-scheme (S-scheme) heterojunction concept was proposed by Yu *et al* [90], which illustrates the charge transfer route clearly and vividly.

Typically, S-scheme heterojunction system comprises two n-type semiconductor photocatalysts with staggered band structure. As shown in figure 11, SC 1 and SC 2 represent oxidation photocatalyst with more positive VB position and reduction photocatalyst with more negative CB position, respectively. When SC 1 and SC 2 come into contact, e- in SC 2 with higher Fermi level could transfer to SC 1 across their interface, thereby forming an interfacial internal electric field and its direction is from SC 2 to SC 1. In addition, the alignment of the Fermi levels of SC 1 and SC 2 to the same level after contact leads to an upward and downward shift in the Fermi levels of SC 1 and SC 2, respectively [91, 92]. Under irradiation, the internal electric field and the band bending offer a driving forces to accelerate the recombination of the useless photoinduced e- of SC 2 and h^+ of SC 1, meanwhile useful e- and h^+ with higher redox ability are remained

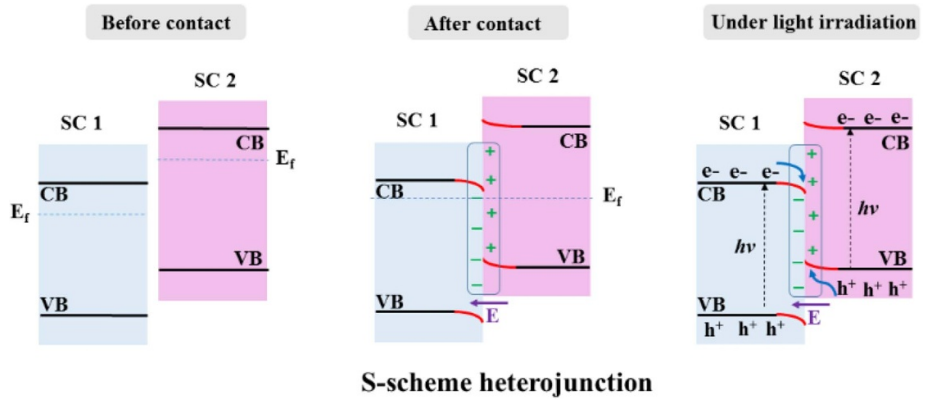

Figure 11. Schematic illustration of the charge transfer pathway in S-scheme heterojunction.

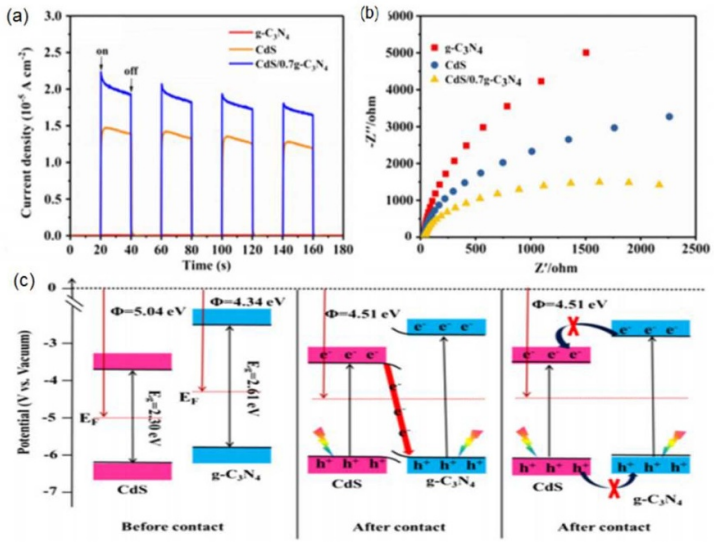

Figure 12. (a) Transient photocurrent response, (b) EIS Nyquist plots of g-C_3N_4, CdS, and CdS/g-C_3N_4, (c) The charge separation pathway in CdS/g-C_3N_4 system (adapted from Li *et al*) [97].

in the CB of SC 2 and in the VB of SC 1, respectively, resulting in a spatial separation of photoinduced charge carriers [93–96]. In S-scheme heterojunction, the charge transfer route is like a 'step' type from macroscopic viewpoint. Such heterojunction system can greatly promote charge separation and acquire strong photoredox ability.

As a typical n-type semiconductor with unique structural properties, g-C_3N_4 can be manipulated to construct efficient g-C_3N_4-based S-scheme heterojunction systems for photocatalytic H_2 production. For instance, Li *et al* [97] reported a novel CdS/g-C_3N_4 S-scheme heterojunction photocatalyst with 2D-2D surface contact prepared by *in situ* hydrothermal growth of CdS nanosheets on g-C_3N_4 nanosheets. It was found that the work function of CdS (5.04 eV) is larger than that of g-C_3N_4 (4.34 eV), which induces the formation of internal electric field and band-edge bending at the interface of the two photocatalysts. This internal electric field promotes the charge carriers separation and diffusion as illustrated in figures 12(a) and (b). Moreover, the formed electric field directing from g-C_3N_4 to CdS thermodynamically facilitates the migration of e- from the CB of CdS to VB of g-C_3N_4 and prevents h^+ in the VB of CdS to diffuse into the VB of g-C_3N_4 and e- in the CB of g-C_3N_4 to diffuse into the CB of CdS, giving rise to an S-scheme system (figure 12(c)). As a result, the CdS/g-C_3N_4 photocatalysts showed a superior photocatalytic H_2 evolution rate, which is about 3060 times higher than that of pristine g-C_3N_4. In addition, Yu *et al* [90] reported the construction of 2D-2D WO_3/g-C_3N_4 S-scheme heterojunction photocatalyst via an electrostatic self-assembly process, which showed an excellent photocatalytic performance towards H_2 generation. Theoretical calculations and band diagram analysis along with *in situ* EPR results confirm a S-scheme charge transfer pathway for WO_3/g-C_3N_4 heterojunction system. Owing to this unique charge transfer route, the photogenerated charge

Table 2. Photocatalytic H_2 generation over g-C_3N_4-based S-scheme heterojunction photocatalysts under visible light illumination.

Heterojunction systems	Fabrication strategy	H_2 production Activity (μmol h^{-1} g^{-1})	Reference (Year)
WO_3/g-C_3N_4	Self-assembly	982	[90] (2019)
CdS/g-C_3N_4	*In-situ* hydrothermal	1530	[97] (2019)
MCN/UCN	Hydrothermal-calcination	598	[98] (2019)
$CuInS_2$@C_3N_4	One-step hydrothermal	373	[99] (2020)
g-C_3N_4/$Zn_{0.2}Cd_{0.8}S$-DETA	*in-situ* growth method	6690	[100] (2020)

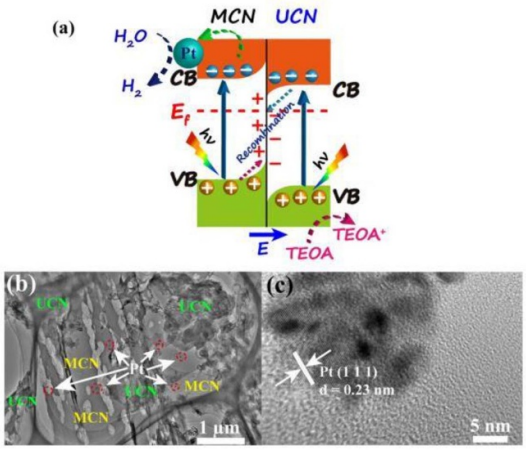

Figure 13. (a) The charge separation pathway in MCN/UCN heterojunction photocatalyst, (b) TEM, (c) HRTEM images of 1 wt% Pt deposited on MCN/UCN (adapted from Ma *et al*) [98].

carriers with strong redox abilities are spatially separated and reserved, contributing to the excellent photocatalytic performance.

Recently, Ma *et al* [98] reported the construction of a novel S-scheme MCN/UCN isotope heterojunction by using melamine and urea as g-C_3N_4 precursors. It was found that H_2 generation rate of optimum MCN/UCN is almost 5.5 and 1.8-fold higher than those of MCN and UCN, respectively, with adding Pt NPs as cocatalyst. The mechanism study shows that the improved photocatalytic activity mainly results from the effective charges separation driven by the internal electric field that formed at the interface of MCN and UCN. Under illumination, the useless e^- from the CB of UCN recombine with the photogenerated holes from the VB of MCN due to the formed electric field at the interface, while the reserved e^- in the CB of MCN further diffuse to Pt NPs for conducting water reduction reaction (figure 13(a)). Additionally, the TEM results (figures 13(b) and (c)) confirm that most Pt NPs are located at MCN surface, indicating that MCN surface is the electron-rich region, which further confirms the S-scheme mechanism. Various g-C_3N_4-based S-scheme heterojunction photocatalysts for H_2 generation reported in recent years are listed in table 2.

The examples mentioned above showed that S-scheme heterojunction systems possess strong redox abilities with thermodynamic advantages in photocatalytic water splitting for H_2 generation, however, as is known, photocatalytic reactions are not only affected by thermodynamics, but also by dynamics. Thus, the thermodynamic advantages of S-scheme heterojunction systems are not sufficient. Highly efficient g-C_3N_4-based S-scheme heterojunction systems may be achieved by employing some strategies such as doping, which is indispensable to adjust and widen the Fermi level difference between the two semiconductors constructing S-scheme heterojunction. Moreover, cocatalyst loading is an effective approach to promote the charge separation and decrease the kinetic barrier of the photocatalytic reaction.

2.4. Metal/g-C_3N_4 schottky junction systems

Hybridization of g-C_3N_4 with metal nanoparticles is also an attractive strategy for improving its photocatalytic properties [101–104]. In principle, when a metal comes into close contact with a semiconductor, a potential difference called Schottky barrier and a depletion layer will be created at the interface between the metal and the semiconductor due to their different work functions and Fermi levels. The Schottky barrier, which can serve as an effective electron skin, prohibits the charge carriers' recombination and prolongs the lifespan of the electrons [105, 106]. For photocatalytic hydrogen evolution reaction, platinum Pt is the most used co-catalyst [107–112]. Liu and co-workers [110] have synthesized Pt/g-C_3N_4 by photodeposition of Pt onto g-C_3N_4 surface, which displayed a H_2 generation activity of

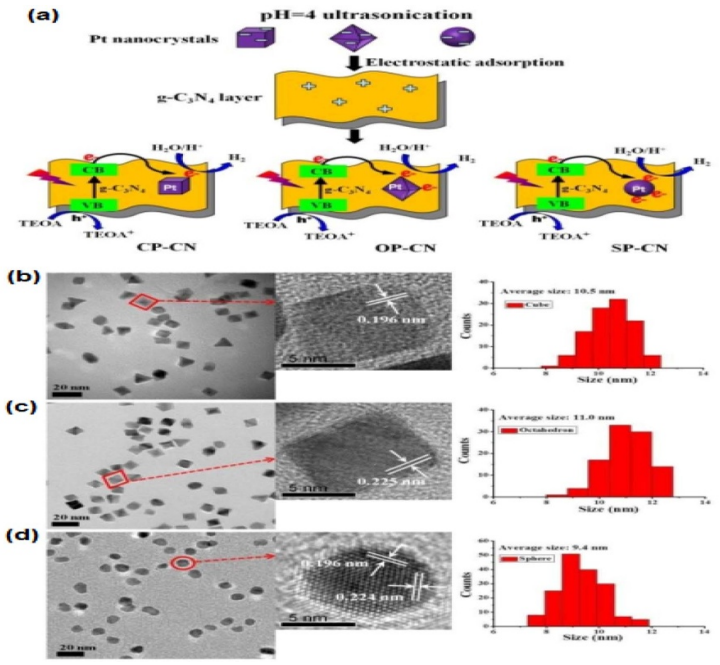

Figure 14. (a) Preparation scheme of Pt/g-C_3N_4 samples, TEM, HRTEM images and size distributions of (b) cubic Pt/g-C_3N_4, (c) octahedral Pt/g-C_3N_4, (d) spherical Pt/g-C_3N_4 (adapted from Cao *et al*) [112].

4210.7 μmol g^{-1} h^{-1}. In the Pt/g-C_3N_4 system, the e^- excited from the CB of g-C_3N_4 will move to the surface of Pt, leading to efficient charge separation and enhanced photoactivity for H_2 generation.

It has been found that Pt NPs size can significantly influences the hydrogen evolution rate of Pt/g-C_3N_4 photocatalyst. In our previous work [111], we studied the photocatalytic activity of Pt/g-C_3N_4 in hydrogen production with different sizes of Pt NPs from single atoms to nano-clusters. The obtained results indicated that single-atom Pt exhibits superior photoactivity compared to nano-clusters Pt. Particularly, single-atom Pt can provide the most abundant active sites and enable maximum accessibility of Pt atoms leading to the highest reaction efficiency. Moreover, it has been proved that the shape of Pt nanoparticle greatly influences the hydrogen generation activity of Pt/g-C_3N_4 system. Cao *et al* [112] reported the construction of Pt/g-C_3N_4 with Pt of different shapes by a colloidal adsorption-deposition method for photocatalytic H_2 production (figure 14(a)). As illustrated in figures 14(b)–(d), TEM and HRTEM images confirm the successful deposition of 3 types of Pt NPs (nanocubes, nanooctahedrals and nanospheres) onto g-C_3N_4 surface. The Pt NPs have similar sizes of about 10 nm, however they exposed different facets. Interestingly, the Pt/g-C_3N_4 hybrids with spherical Pt nanoparticle shape exhibited the highest photocatalytic hydrogen generation activity owing to its favorable exposed facets.

Because of the high costs of Pt noble metal, considerable efforts have been made to reduce its amount of usage with maintaining its excellent activity for photocatalytic H_2 production via replacing a part of Pt with transition metals [113–116]. In light of this, Han *et al* [116] synthesized Pt-Co/g-C_3N_4 by *in-situ* chemical deposition method, which showed hydrogen generation activity of 960 μmol h^{-1} g^{-1} better than that of Pt/g-C_3N_4. The increased hydrogen production efficiency is attributed to the synergistic effect between Pt and Co, which modifies the Fermi level position of Pt-Co alloy co-catalyst in comparison to Pt, resulting in improved electron trapping ability of the Pt-Co co-catalyst and thus enhancing the photocatalytic efficiency. In order to prepare cost-effective CNBH photocatalysts for hydrogen generation, loading carbon nitride with non-noble-metals, which are low-cost and abundant elements, has also been explored [117–120]. Recently, Han *et al* [120] found that loading g-C_3N_4 with Ni-Mo alloy resulted in improved hydrogen production activity of 1785 μmol h^{-1} g^{-1}, which is close to Pt/g-C_3N_4 photoactivity. This work demonstrates the successful Pt-free approach for photocatalytic H_2 production.

3. Conclusions and prospects

In this mini review, the recent advancements in g-C_3N_4 based heterojunctions for H_2 production via photocatalytic water splitting have been reviewed. Over the past two decades, various types of CNBH systems have been explored as photocatalysts in photocatalytic hydrogen generation. Up to now, the construction of CNBH could effectively improve the efficiency of photocatalytic systems. However, despite the considerable

progress achieved in this field, the existing apparent quantum efficiency and water splitting efficiency (STH) by g-C_3N_4 based heterojunctions are still far from satisfactory. As such, coupling g-C_3N_4 with low bandgap materials such as black phosphorus and WS_2, etc could achieve better usage of solar energy and attain a high quantum efficiency.

With type-II and Z-scheme heterojunction systems, there is still much vagueness in the charge transfer mechanism and it maybe different from what it is claimed to be. Therefore, it is necessary to clarify and understand the interfacial charges transfer pathway. Besides direct experimental support by ultrafast spectroscopic studies, in this regard, DFT computation should also be well developed and applied to further understand and clarify the charges transfer pathway and even the mechanism of photocatalytic reaction over g-C_3N_4-based heterojunctions photocatalysts.

In order to overcome the shortcomings of type II and Z-scheme heterojunction, S-scheme heterojunction concept was proposed, which explains and illustrates the charge transfer process clearly and vividly. S-scheme system enables high charges redox ability and efficient charge separation, resulting in boosted photocatalytic performance. Despite considerable progress has been achieved in C_3N_4-based heterojunction photocatalysts, S-scheme heterojunction system is still at the primary stage of study. In the hopeful future, highly efficient g-C_3N_4-based S-scheme heterojunction systems can be methodically realized by employing some strategies such as doping and co-catalyst loading. Furthermore, to make g-C_3N_4 a cost effective photocatalyst the application of non-noble metal as co-catalyst should be further investigated.

Acknowledgments

This work was supported by the National Natural Science Foundation of China (21976116), Shaanxi Science and Technology Program (2020KWZ-005), SAFEA of China (High-end Foreign Expert Project), Alexander-von-Humboldt Foundation of Germany (Group-Linkage Program).

ORCID iDs

Baker Rhimi https://orcid.org/0000-0003-0203-9120
Chuanyi Wang https://orcid.org/0000-0002-7146-115X

References

[1] Armaroli N and Balzani V 2007 The future of energy supply: challenges and opportunities *Chem.-Int. Ed.* **46** 52–66
[2] Kudo A and Miseki Y 2009 Heterogeneous photocatalyst materials for water splitting *Chem. Soc. Rev.* **38** 253–78
[3] Kabir E, Kumar P, Kumar S, Adelodun A A and Kim K H 2018 Solar energy: potential and future prospects *Renewable Sustainable Energy Rev.* **82** 894–900
[4] Fujishima A and Honda K 1972 Photolysis-decomposition of water at the surface of an irradiated semiconductor *Nature* **238** 37–38
[5] Choi S K, Yang H S, Kim J H and Park H 2012 Organic dye-sensitized TiO_2 as a versatile photocatalyst for solar hydrogen and environmental remediation *Appl. Catal.* B **121** 206–13
[6] Liu D, Zhang S, Wang J, Peng T and Li R 2019 Direct Z-scheme 2D/2D photocatalyst based on ultrathin g-C_3N_4 and WO_3 nanosheets for efficient visible-light-driven H_2 generation *ACS Appl. Mater. Interfaces* **11** 27913–23
[7] Zhu C, Liu C, Fu Y, Gao J, Huang H, Liu Y and Kang Z 2019 Construction of CDs/CdS photocatalysts for stable and efficient hydrogen production in water and seawater *Appl. Catal.* B **242** 178–85
[8] Wang Q, Lian J, Li J, Wang R, Huang H, Su B and Lei Z 2015 Highly efficient photocatalytic hydrogen production of flower-like cadmium sulfide decorated by histidine *Sci. Rep.* **5** 13593
[9] Patnaik S, Martha S and Parida K M 2016 An overview of the structural, textural and morphological modulations of g-C_3N_4 towards photocatalytic hydrogen production *RSC Adv.* **6** 46929–51
[10] Ren Y, Zeng D and Ong W J 2019 Interfacial engineering of graphitic carbon nitride (g-C_3N_4)-based metal sulfide heterojunction photocatalysts for energy conversion: A review *Chin. J. Catal.* **40** 289–319
[11] Wang X, Maeda K, Thomas A, Takanabe K, Xin G, Carlsson J M, Domen K and Antonietti M 2009 A metal-free polymeric photocatalyst for hydrogen production from water under visible light *Nat. Mater.* **8** 76–80
[12] Liu J, Wang H and Antonietti M 2016 Graphitic carbon nitride "reloaded": emerging applications beyond (photo)catalysis *Chem. Soc. Rev.* **45** 2308–26
[13] Wen J, Xie J, Chen X and Li X 2017 A review on g-C_3N_4-based photocatalysts *Appl. Surf. Sci.* **391** 72–123
[14] Dong G, Ho W, Li Y and Zhang L 2015 Facile synthesis of porous graphene-like carbon nitride ($C_6N_9H_3$) with excellent photocatalytic activity for NO removal *Appl. Catal.* B **174—175** 477–85
[15] Li G, Lian Z, Wang W, Zhang D and Li H 2016 Nanotube confinement induced size-controllable g-C_3N_4 quantum dots modified single-crystalline TiO_2 nanotube arrays for stable synergetic photoelectrocatalysis *Nano Energy* **19** 446–54
[16] Wang D H, Pan J N, Li H H, Liu J J, Wang Y B, Kang L T and Yao J N 2016 A pure organic heterostructure of μ-oxo dimeric iron(III) porphyrin and graphitic-C_3N_4 for solar H_2 roduction from water *J. Mater. Chem.* A **4** 290–6
[17] Zhang Z, Jiang D, Li D, He M and Chen M 2016 Construction of $SnNb_2O_6$ nanosheet/g-C_3N_4 nanosheet two-dimensional heterostructures with improved photocatalytic activity: synergistic effect and mechanism insight *Appl. Catal.* B **183** 113–23
[18] Xiao J, Xie Y, Nawaz F, Wang Y, Du P and Cao H 2016 Dramatic coupling of visible light with ozone on honeycomb-like porous gC_3N_4 towards superior oxidation of water pollutants *Appl. Catal.* B **183** 417–25

[19] Liu J, Wang H, Chen Z P, Moehwald H, Fiechter S, van de Krol R, Wen L, Jiang L and Antonietti M 2015 Microcontact-printing assisted access of graphitic carbon nitride films with favorable textures toward photoelectrochemical application *Adv. Mater.* **27** 712–8

[20] Shiraishi Y, Kofuji Y, Sakamoto H, Tanaka S, Ichikawa S and Hirai T 2015 Effects of surface defects on photocatalytic H_2O_2 production by mesoporous graphitic carbon nitride under visible light irradiation *ACS Catal.* **5** 3058–66

[21] Sun S and Liang S 2017 Recent advances in functional mesoporous graphitic carbon nitride (mpg-C_3N_4) polymers *Nanoscale* **9** 10544–78

[22] Wang X L and Yang H G 2017 Facile fabrication of high-yield graphitic carbon nitride with a large surface area using bifunctional urea for enhanced photocatalytic performance *Appl. Catal.* B **205** 624–30

[23] Ye C, Li J X, Li Z J, Li X B, Fan X B, Zhang L P, Chen B, Tung C H and Wu L Z 2015 Enhanced driving force and charge separation efficiency of protonated g-C_3N_4 for photocatalytic O_2 evolution *ACS Catal.* **5** 6973–9

[24] Jiang L, Yuan X, Pan Y, Liang J, Zeng G, Wu Z and Wang H 2017 Doping of graphitic carbon nitride for photocatalysis: a review *Appl. Catal.* B **217** 388–406

[25] Li X, Zhang J, Zhou F, Zhang H, Bai J, Wang Y and Wang H 2018 Preparation of N-vacancy-doped g-C_3N_4 with outstanding photocatalytic H_2O_2 production ability by dielectric barrier discharge plasma treatment *Chin. J. Catal.* **39** 1090–8

[26] Lin Z and Wang X 2013 Nanostructure engineering and doping of conjugated carbon nitride semiconductors for hydrogen photosynthesis *Angew. Chem. Int. Ed.* **52** 1735–8

[27] Zhang M, Duan Y, Jia H, Wang F, Wang L, Su Z and Wang C 2017 Defective graphitic carbon nitride synthesized by controllable co-polymerization with enhanced visible light photocatalytic hydrogen evolution *Catal. Sci. Technol.* **7** 452–8

[28] Chen X, Zhao X, Kong Z, Ong W J and Li N 2018 Unravelling the electrochemical mechanisms for nitrogen fixation on single transition metal atoms embedded in defective graphitic carbon nitride *J. Mater. Chem.* A **6** 21941–8

[29] Kong Z, Chen X, Ong W J, Zhao X and Li N 2019 Atomic-level insight into the mechanism of 0D/2D black phosphorus quantum dot/graphitic carbon nitride (BPQD/GCN) metal-free heterojunction for photocatalysis *Appl. Surf. Sci.* **463** 1148–53

[30] Zeng D, Wu P, Ong W J, Tang B, Wu M, Zheng H, Chen Y and Peng D L 2018 Construction of network-like and flower-like 2H-$MoSe_2$ nanostructures coupled with porous g-C_3N_4 for noble-metal-free photocatalytic H_2 evolution under visible light *Appl. Catal.* B **233** 26–34

[31] Zeng D, Ong W J, Zheng H, Wu M, Chen Y, Peng D L and Han M Y 2017 $Ni_{12}P_5$ nanoparticles embedded into porous gC_3N_4 nanosheets as a noble-metal-free hetero-structure photocatalyst for efficient H_2 production under visible light *J. Mater. Chem.* A **5** 16171–8

[32] Du X, Yi X, Wang P, Deng J and Wang C C 2019 Enhanced photocatalytic Cr(VI) reduction and diclofenac sodium degradation under simulated sunlight irradiation over MIL-100(Fe)/g-C_3N_4 heterojunctions *Chin. J. Catal.* **40** 70–79

[33] Jing L, Ong W J, Zhang R, Pickwell-macpherson E and Yu J C 2018 Graphitic carbon nitride nanosheet wrapped mesoporous titanium dioxide for enhanced photoelectrocatalytic water splitting *Catal. Today* **315** 103–9

[34] Ong W J, Tan L L, Ng Y H, Yong S T and Chai S P 2016 Graphitic carbon nitride (g-C_3N_4)-based photocatalysts for artificial photosynthesis and environmental remediation: are we a step closer to achieving sustainability? *Chem. Rev.* **116** 7159–329

[35] Li X, Yu J and Jaroniec M 2016 Hierarchical photocatalysts *Chem. Soc. Rev.* **45** 2603–36

[36] Jafari T, Moharreri E, Amin A S, Miao R, Song W and Suib S L 2016 Photocatalytic water splitting–the untamed dream: a review of recent advances *Molecules* **21** 900

[37] Murugesan P, Moses J A and Anandharamakrishnan C 2019 Photocatalytic disinfection efficiency of 2D structure graphitic carbon nitride-based nanocomposites: a review *J. Mater. Sci.* **54** 12206–35

[38] Mamba G and Mishra A K 2016 Graphitic carbon nitride (g-C_3N_4) nanocomposites: a new and exciting generation of visible light driven photocatalysts for environmental pollution remediation *Appl. Catal.* B **198** 347–77

[39] Zhang S, Gu P, Ma R, Luo C, Wen T, Zhao G, Cheng W and Wang X 2019 Recent developments in fabrication and structure regulation of visible-light-driven g-C_3N_4-based photocatalysts towards water purification: a critical review *Catal. Today* **335** 65–77

[40] Zhang Z and Yates Jr J T 2012 Band bending in semiconductors: chemical and physical consequences at surfaces and interfaces *Chem. Rev.* **112** 5520–51

[41] Wang H, Zhang L, Chen Z, Hu J, Li S, Wang Z, Liu J and Wang X 2014 Semiconductor heterojunction photocatalysts: design, construction, and photocatalytic performances *Chem. Soc. Rev.* **43** 5234–44

[42] Huang D, Yan X, Yan M, Zeng G, Zhou C, Wan J, Cheng M and Xue W 2018 Graphitic carbon nitride-based heterojunction photoactive nanocomposites: applications and mechanism insight *ACS Appl. Mater. Interfaces* **10** 21035–55

[43] Fu J, Yu J, Jiang C and Cheng B 2017 g-C_3N_4- based heterostructured photocatalysts *Adv. Energy Mater.* **8** 1701503

[44] Shen L, Xing Z, Zou J, Li Z, Wu X, Zhang Y, Zhu Q, Yang S and Zhou W 2017 Black TiO_2 nanobelts/g-C_3N_4 nanosheets laminated heterojunctions with efficient visible-light-driven photocatalytic performance *Sci. Rep.* **7** 41978

[45] Lin Y, Shi H, Jiang Z, Wang G, Zhang X, Zhu H, Zhang R and Zhu C 2017 Enhanced optical absorption and photocatalytic H_2 production activity of g-C_3N_4/TiO_2 heterostructure by interfacial coupling: A DFT+ U study *Int. J. Hydrogen Energy* **42** 9903–13

[46] Liu L, Qi Y, Hu J, Liang Y and Cui W 2015 Efficient visible-light photocatalytic hydrogen evolution and enhanced photostability of core@ shell Cu_2O@ g-C_3N_4 octahedra *Appl. Surf. Sci.* **351** 1146–54

[47] Wang J, Guan Z, Huang J, Li Q and Yang J 2014 Enhanced photocatalytic mechanism for the hybrid gC_3N_4/MoS_2 nanocomposite *J. Mater. Chem.* A **2** 7960–6

[48] Yuming T, Lei G, Wang K and Yuesheng C 2014 Synthesis of novel MoS_2/g-C_3N_4 heterojunction photocatalysts with enhanced hydrogen evolution activity *Mater. Charact.* **87** 70–73

[49] Cao S W, Liu X F, Yuan Y P, Zhang Z Y, Liao Y S, Fang J, Loo S C J, Sum T C and Xue C 2014 Solar-to-fuels conversion over In_2O_3/g-C_3N_4 hybrid photocatalysts *Appl. Catal.* B **147** 940–6

[50] Qu A, Xu X, Xie H, Zhang Y, Li Y and Wang J 2016 Effects of calcining temperature on photocatalysis of g-C_3N_4/TiO_2 composites for hydrogen evolution from water *Mater. Res. Bull.* **80** 167–76

[51] Zou Y, Shi J W, Ma D, Fan Z, Lu L and Niu C 2017 In situ synthesis of C-doped TiO_2@ g-C_3N_4 core-shell hollow nanospheres with enhanced visible-light photocatalytic activity for H_2 evolution *Chem. Eng. J.* **322** 435–44

[52] Tan S, Xing Z, Zhang J, Li Z, Wu X, Cui J, Kuang J, Zhu Q and Zhou W 2018 Ti^{3+}-TiO_2/g-C_3N_4 mesostructured nanosheets heterojunctions as efficient visible-light-driven photocatalysts *J. Catal.* **357** 90–99

[53] Pan J, Dong Z, Wang B, Jiang Z, Zhao C, Wang J, Song C, Zheng Y and Li C 2019 The enhancement of photocatalytic hydrogen production via Ti^{3+} self-doping black TiO_2/g-C_3N_4 hollow core-shell nano-heterojunction *Appl. Catal.* B **242** 92–99

[54] Hao X, Zhou J, Cui Z, Wang Y, Wang Y and Zou Z 2018 Zn-vacancy mediated electron-hole separation in ZnS/g-C_3N_4 heterojunction for efficient visible-light photocatalytic hydrogen production *Appl. Catal.* B **229** 41–51

[55] Li J, Yin Y, Liu E, Ma Y, Wan J, Fan J and Hu X 2017 In situ growing Bi_2MoO_6 on g-C_3N_4 nanosheets with enhanced photocatalytic hydrogen evolution and disinfection of bacteria under visible light irradiation *J. Hazard. Mater.* **321** 183–92

[56] Wang B, Zhang J and Huang F 2017 Enhanced visible light photocatalytic H_2 evolution of metal-free g-C_3N_4/SiC heterostructured photocatalysts *Appl. Surf. Sci.* **391** 449–56

[57] Waqas M, Yang B, Cao L, Zhao X, Iqbal W, Xiao K, Zhu C and Zhang J 2019 Tuning the N-bonded cerium (iii) fraction/gC_3N_4 interface in hollow structures using an in situ reduction treatment for superior photochemical hydrogen evolution *Catal. Sci. Technol.* **9** 5322–32

[58] Zhu Y, Wan T, Wen X, Chu D and Jiang Y 2019 Tunable Type I and II heterojunction of CoO_x nanoparticles confined in g-C_3N_4 nanotubes for photocatalytic hydrogen production *Appl. Catal.* B **244** 814–22

[59] Zheng D, Zhang G and Wang X 2015 Integrating CdS quantum dots on hollow graphitic carbon nitride nanospheres for hydrogen evolution photocatalysis *Appl. Catal.* B **179** 479–88

[60] Zhang J, Wang Y, Jin J, Zhang J, Lin Z, Huang F and Yu J 2013 Efficient visible-light photocatalytic hydrogen evolution and enhanced photostability of core/shell CdS/g-C_3N_4 nanowires *ACS Appl. Mater. Interfaces* **5** 10317–24

[61] Li S, Zhang M, Qu Z, Cui X, Liu Z, Piao C, Li S, Wang J and Song Y 2020 Fabrication of highly active Z-scheme Ag/g-C_3N_4-Ag-Ag_3PO_4 (1 1 0) photocatalyst photocatalyst for visible light photocatalytic degradation of levofloxacin with simultaneous hydrogen production *Chem. Eng. J.* **382** 122394

[62] Ding X, Li Y, Zhao J, Zhu Y, Li Y, Deng W and Wang C 2015 Enhanced photocatalytic H_2 evolution over CdS/Au/g-C_3N_4 composite photocatalyst under visible-light irradiation *APL Mater.* **3** 104410

[63] Zhao H, Ding X, Zhang B, Li Y and Wang C 2017 Enhanced photocatalytic hydrogen evolution along with byproducts suppressing over Z-scheme $Cd_xZn_{1-x}S$/Au/g-C_3N_4 photocatalysts under visible light *Sci. Bull.* **62** 602–9

[64] Shi F, Chen L, Chen M and Jiang D 2015 A g-C_3N_4/nanocarbon/$ZnIn_2S_4$ nanocomposite: an artificial Z-scheme visible-light photocatalytic system using nanocarbon as the electron mediator *Chem. Commun.* **51** 17144–7

[65] Jo W K and Selvam N C S 2017 Z-scheme CdS/g-C_3N_4 composites with RGO as an electron mediator for efficient photocatalytic H_2 production and pollutant degradation *Chem. Eng. J.* **317** 913–24

[66] Ye R, Fang H, Zheng Y Z, Li N, Wang Y and Tao X 2016 Fabrication of $CoTiO_3$/g-C_3N_4 hybrid photocatalysts with enhanced H_2 evolution: Z-scheme photocatalytic mechanism insight *ACS Appl. Mater. Interfaces* **8** 13879–89

[67] Yu W, Chen J, Shang T, Chen L, Gu L and Peng T 2017 Direct Z-scheme g-C_3N_4/WO_3 photocatalyst with atomically defined junction for H_2 production *Appl. Catal.* B **219** 693–704

[68] She X *et al* 2017 High efficiency photocatalytic water splitting using 2D α-Fe_2O_3/g-C_3N_4 Z-scheme catalysts *Adv. Energy Mater.* **7** 1700025

[69] Idrees F, Dillert R, Bahnemann D, Butt F K and Tahir M 2019 In-situ synthesis of Nb_2O_5/g-C_3N_4 heterostructures as highly efficient photocatalysts for molecular H_2 evolution under solar illumination *Catalysts* **9** 169

[70] Huang Z F, Song J, Wang X, Pan L, Li K, Zhang X, Wang L and Zou J J 2017 Switching charge transfer of C_3N_4/$W_{18}O_{49}$ from type-II to Z-scheme by interfacial band bending for highly efficient photocatalytic hydrogen evolution *Nano Energy* **40** 308–16

[71] Yang C W, Xue Z, Qin J Q, Sawangphruk M, Rajendran S, Zhang X Y and Liu R P 2019 Visible light-driven photocatalytic H_2 generation and mechanism insights into $Bi_2O_2CO_3$/GC_3N_4 Z-scheme photocatalyst *J. Phys. Chem.* C **123** 4795–804

[72] Han X, Xu D, An L, Hou C, Li Y, Zhang Q and Wang H 2018 WO_3/g-C_3N_4 two-dimensional composites for visible-light driven photocatalytic hydrogen production *Int. J. Hydrogen Energy* **43** 4845–55

[73] Jo W K, Moru S and Tonda S 2020 Magnetically responsive $SnFe_2O_4$/g-C_3N_4 hybrid photocatalysts with remarkable visible-light-induced performance for degradation of environmentally hazardous substances and sustainable hydrogen production *Appl. Surf. Sci.* **506** 144939

[74] Liu Y, Liu H, Zhou H, Li T and Zhang L 2019 A Z-scheme mechanism of N-ZnO/g-C_3N_4 for enhanced H_2 evolution and photocatalytic degradation *Appl. Surf. Sci.* **466** 133–40

[75] Zhang R, Bi L, Wang D, Lin Y, Zou X and Xie T 2020 Investigation on various photo-generated carrier transfer processes of SnS_2/g-C_3N_4 heterojunction photocatalysts for hydrogen evolution *J. Colloid Interface Sci.* **578** 431-40

[76] Wang J, Xia Y, Zhao H, Wang G, Xiang L, Xu J and Komarneni S 2017 Oxygen defects-mediated Z-scheme charge separation in g-C_3N_4/ZnO photocatalysts for enhanced visible-light degradation of 4-chlorophenol and hydrogen evolution *Appl. Catal.* B **206** 406–16

[77] Afroz K, Moniruddin M, Bakranov N, Kudaibergenov S and Nuraje N 2018 Heterojunctions of halogen-doped carbon nitride nanosheets and BiOI for sunlight-driven water-splitting *J. Mater. Chem.* A **6** 21696–718

[78] Zhou P, Yu J and Jaroniec M 2014 All-solid-state Z-scheme photocatalytic systems *Adv. Mater.* **26** 4920–35

[79] Wan X, Liu G, Chen Z G, Li F, Wang L, Lu G Q and Cheng H M 2009 Enhanced photocatalytic hydrogen evolution by prolonging the lifetime of carriers in ZnO/CdS heterostructures *Chem. Commun.* 3452–4

[80] Hanna M C and Nozik A J 2006 Solar conversion efficiency of photovoltaic and photoelectrolysis cells with carrier multiplication absorbers *J. Phys. D: Appl. Phys.* **100** 074510

[81] Wang X, Liu G, Wang L, Chen Z G, Lu G Q and Cheng H M 2012 ZnO–CdS@Cd heterostructure for effective photocatalytic hydrogen generation *Adv. Energy Mater.* **2** 42–46

[82] Sasaki Y, Kato H and Kudo A 2013 $[Co(bpy)_3]^{3+/2+}$ and $[Co(phen)_3]^{3+/2+}$ electron mediators for overall water splitting under sunlight irradiation using Z-scheme photocatalyst system *J. Am. Chem. Soc.* **135** 5441–9

[83] Maeda K, Lu D and Domen K 2013 Solar-Driven Z-scheme Water Splitting Using Modified $BaZrO_3$–$BaTaO_2N$ Solid Solutions as Photocatalysts *ACS Catal.* **3** 1026–33

[84] Chen S, Qi Y, Hisatomi T, Ding Q, Asai T, Li Z, Ma S S K, Zhang F, Domen K and Li C 2015 Efficient visible-light-driven Z-scheme overall water splitting using a $MgTa_2O_{6-x}N_y$/TaON heterostructure photocatalyst for H_2 evolution *Angew. Chem., Int. Ed.* **54** 8498–501

[85] Yu J, Wang S, Low J and Xiao W 2013 Enhanced photocatalytic performance of direct Z-scheme g-C_3N_4–TiO_2 photocatalysts for the decomposition of formaldehyde in air *Phys. Chem. Chem. Phys.* **15** 16883–90

[86] Low J, Yu J, Jaroniec M, Wageh S and Al-Ghamdi A A 2017 Heterojunction photocatalysts *Adv. Mater.* **29** 1601694

[87] Sasaki Y, Nemoto H, Saito K and Kudo A 2009 Solar water splitting using powdered photocatalysts driven by Z-schematic interparticle electron transfer without an electron mediator *J. Phys. Chem.* C **113** 17536–42

[88] Jia Q, Iwase A and Kudo A 2014 $BiVO_4$–Ru/$SrTiO_3$: rh composite Z-scheme photocatalyst for solar water splitting *Chem. Sci.* **5** 1513–9

[89] Xu Q, Zhang L, Yu J, Wageh S, Al-Ghamdi A A and Jaroniec M 2018 Direct Z-scheme photocatalysts: principles, synthesis, and applications *Mater. Today* **21** 1042–63

[90] Fu J W, Xu Q L, Low J X, Jiang C J and Yu J G 2019 Ultrathin 2D/2D WO_3/g-C_3N_4 step scheme H_2-production photocatalyst *Appl. Catal.* B **243** 556–65

[91] Xia P, Cao S, Zhu B, Liu M, Shi M, Yu J and Zhang Y 2020 Designing 0D/2D S-scheme heterojunction over polymeric carbon nitride for visible-light photocatalytic inactivation of bacteria *Angew. Chem. Int. Ed.* **59** 52183–25

[92] Xu Q, Zhang L, Cheng B, Fan J and Yu J 2020 S-scheme heterojunction photocatalyst *Chem* **6** 1543–59

[93] Xie Q, He W, Liu S, Li C, Zhang J and Wong P K 2020 Bifunctional S-scheme g-C_3N_4/Bi/$BiVO_4$ hybrid photocatalysts toward artificial carbon cycling *Chin. J. Catal.* **41** 140–53

[94] Wang J, Zhang Q, Deng F, Luo X and Dionysiou D D 2020 Rapid toxicity elimination of organic pollutants by the photocatalysis of environment-friendly and magnetically recoverable step-scheme $SnFe_2O_4$/$ZnFe_2O_4$ nano-heterojunction *Chem. Eng. J.* **379** 122264

[95] Jia X, Han Q, Zheng M and Bi H 2019 One pot milling route to fabricate step-scheme AgI/I-BiOAc photocatalyst: energy band structure optimized by the formation of solid solution *Appl. Surf. Sci.* **489** 409–19

[96] Gong H, Hao X, Jin Z and Ma Q 2019 WP modified S-scheme $Zn_{0.5}Cd_{0.5}S$/WO_3 for efficient photocatalytic hydrogen production *New J. Chem.* **43** 19159–71

[97] Ren D, Zhang W, Ding Y, Shen R, Jiang Z, Lu X and Li X 2019 In situ fabrication of robust cocatalyst-free CdS/g-C_3N_4 2D–2D step-scheme heterojunctions for highly active H_2 evolution *Sol. RRL* **4** 1900423

[98] Xu Q, Ma D, Yang S, Tian Z, Cheng B and Fan J 2019 Novel g-C_3N_4/g-C_3N_4 S-scheme isotype heterojunction for improved photocatalytic hydrogen generation *Appl. Surf. Sci.* **495** 143555

[99] Luo J, Lin Z, Zhao Y, Jiang S and Song S 2020 The embedded $CuInS_2$ into hollow-concave carbon nitride for photocatalytic H_2O splitting into H_2 with S-scheme principle *Chin. J. Catal.* **41** 122–30

[100] Mei F, Li Z, Dai K, Zhang J and Liang C 2020 Step-scheme porous g-C_3N_4/$Zn_{0.2}Cd_{0.8}S$-DETA composites for efficient and stable photocatalytic H_2 production *Chin. J. Catal.* **41** 41–49

[101] Liu H, Liu X Y, Yang W W, Shen M Q, Geng S, Yu C, Shen B and Yu Y S 2019 Photocatalytic dehydrogenation of formic acid promoted by a superior PdAg@gC_3N_4 Mott–Schottky heterojunction *J. Mater. Chem.* A **7** 2022–6

[102] Li Z, Ma Y N, Hu X Y, Liu E Z and Fan J 2019 Enhanced photocatalytic H_2 production over dual-cocatalyst-modified g-C_3N_4 heterojunctions *Chin. J. Catal.* **40** 434–45

[103] Wei Z D, Liu J Y, Fang W J, Guo W Q, Zhu Y, Xu M Q, Jiang Z and Shangguan W F 2019 Photocatalytic hydrogen energy evolution from antibiotic wastewater via metallic bi nanosphere doped g-C_3N_4: performances and mechanisms *Catal. Sci. Technol.* **9** 5279–91

[104] Su T M, Hood Z D, Naguib M, Bai L, Luo S, Rouleau C M, Ivanov I N, Ji H B, Qin Z Z and Wu Z L 2019 2D/2D heterojunction of Ti_3C_2/gC_3N_4 nanosheets for enhanced photocatalytic hydrogen evolution *Nanoscale* **11** 8138–49

[105] Li G and Gray K A 2007 The solid–solid interface: explaining the high and unique photocatalytic reactivity of TiO_2-based nanocomposite materials *Chem. Phys.* **339** 173–87

[106] Khan M R, Chuana T W, Yousuf A, Chowdhury M N K and Cheng C K 2015 Schottky barrier and surface plasmonic resonance phenomena towards the photocatalytic reaction: study of their mechanisms to enhance photocatalytic activity *Catal. Sci. Technol.* **5** 2522–31

[107] Chen S, Li Y and Wang C 2015 Visible-light-driven photocatalytic H_2 evolution from aqueous suspensions of perylene diimide dye-sensitized Pt/TiO_2 Catalysts *RSC Adv.* **5** 15880–5

[108] Chen S, Wang C, Bunes B R, Li Y, Wang C and Zang L 2015 Enhancement of visible-light-driven photocatalytic H_2 evolution from water over g-C_3N_4 through combination with perylene diimide aggregates *Appl. Catal.* A **498** 63–68

[109] Li X, Bi W, Zhang L, Tao S, Chu W, Zhang Q, Luo Y, Wu C and Xie Y 2016 Single-atom Pt as co-catalyst for enhanced photocatalytic H_2 evolution *Adv. Mater.* **28** 2427–31

[110] Liu M, Xia P, Zhang L, Cheng B and Yu J 2018 Enhanced photocatalytic H_2-production activity of gC_3N_4 nanosheets via optimal photodeposition of Pt as cocatalyst *ACS Sustainable Chem. Eng.* **6** 10472–80

[111] Zhu Y, Wang T, Xu T, Li Y and Wang C 2019 Size effect of Pt co-catalyst on photocatalytic efficiency of g-C_3N_4 for hydrogen evolution *Appl. Surf. Sci.* **464** 36–42

[112] Cao S, Jiang J, Zhu B and Yu J 2016 Shape-dependent photocatalytic hydrogen evolution activity over a Pt nanoparticle coupled gC_3N_4 photocatalyst *Phys. Chem. Chem. Phys.* **18** 19457–63

[113] Sun K, Shen J, Liu Q, Tang H, Zhang M, Zulfiqar S and Lei C 2020 Synergistic effect of Co (II)-hole and Pt-electron cocatalysts for enhanced photocatalytic hydrogen evolution performance of P-doped g-C_3N_4 *Chin. J. Catal.* **41** 72–81

[114] Bi L, Gao X, Ma Z, Zhang L, Wang D and Xie T 2017 Enhanced separation efficiency of $PtNi_x$/g-C_3N_4 for photocatalytic hydrogen production *Chem. Cat. Chem.* **9** 3779-85

[115] Cai H, Wang B, Xiong L, Yang G, Yuan L, Bi J, Yu X, Zhang X, Yang S and Yang S 2020 Bridging effect of Co heteroatom between g-C_3N_4 and Pt NPs for enhanced photocatalytic hydrogen evolution *Chem. Eng. J.* **394** 124964

[116] Han C, Lu Y, Zhang J, Ge L, Li Y, Chen C, Xin Y, Wu L and Fang S 2015 Novel PtCo alloy nanoparticle decorated 2D g-C_3N_4 nanosheets with enhanced photocatalytic activity for H_2 evolution under visible light irradiation *J. Mater. Chem.* A **3** 23274–82

[117] Liu J, Jia Q, Long J, Wang X, Gao Z and Gu Q 2018 Amorphous NiO as co-catalyst for enhanced visible-light-driven hydrogen generation over g-C_3N_4 photocatalyst *Appl. Catal.* B **222** 35–43

[118] Hou Y, Zhu Y, Xu Y and Wang X 2014 Photocatalytic hydrogen production over carbon nitride loaded with WS_2 as cocatalyst under visible light *Appl. Catal.* B **156–157** 122–7

[119] Kong L, Dong Y, Jiang P, Wang G, Zhang H and Zhao N 2016 Light-assisted rapid preparation of a Ni/gC_3N_4 magnetic composite for robust photocatalytic H_2 evolution from water *J. Mater. Chem.* A **4** 9998–10007

[120] Han X, Xu D, An L, Hou C, Li Y, Zhang Q and Wang H 2019 Ni-Mo nanoparticles as co-catalyst for drastically enhanced photocatalytic hydrogen production activity over g-C_3N_4 *Appl. Catal.* B **243** 136–44